

## Article

# Wireless Power Transmission System for Powering Rotating Parts of Automatic Machineries

Vladimir Kindl <sup>1</sup>, Tomas Kavalir <sup>2</sup>, Jiri Sika <sup>2</sup>, Jan Hnatik <sup>2</sup>, Michal Krizek <sup>2</sup> and Michal Frivaldsky <sup>3,\*</sup> <sup>1</sup> Faculty of Electrical Engineering, University of West Bohemia, 306 14 Pilsen, Czech Republic<sup>2</sup> Regional Technological Institute, University of West Bohemia, 306 14 Pilsen, Czech Republic<sup>3</sup> Department of Mechatronics and Electronics (DME), University of Žilina, 010 26 Zilina, Slovakia

\* Correspondence: michal.frivaldsky@feit.uniza.sk; Tel.: +421-41-513-1600

**Abstract:** This paper deals with the analysis of a suitable compensation topology of a wireless power transmission system for powering the rotating parts of modern automatic machine tools. It summarizes the important properties of the serio-parallel compensation topology suitable for this application and demonstrates a detailed mathematical derivation using the first harmonic approximation. The paper details the industrial implementation of the system in a specific automatic machine tool application and demonstrates the strong technical advantages of the proposed design. Important theoretical conclusions and technical assumptions made when considering the system layout are verified by experimental laboratory measurements and the final deployment of the technology in the professional tool DMU 40 eVo linear.

**Keywords:** wireless power transfer; load; efficiency; machine tool



**Citation:** Kindl, V.; Kavalir, T.; Sika, J.; Hnatik, J.; Krizek, M.; Frivaldsky, M. Wireless Power Transmission System for Powering Rotating Parts of Automatic Machineries. *Energies* **2022**, *15*, 6856. <https://doi.org/10.3390/en15186856>

Academic Editor: Alon Kuperman

Received: 18 August 2022

Accepted: 15 September 2022

Published: 19 September 2022

**Publisher's Note:** MDPI stays neutral with regard to jurisdictional claims in published maps and institutional affiliations.



**Copyright:** © 2022 by the authors. Licensee MDPI, Basel, Switzerland. This article is an open access article distributed under the terms and conditions of the Creative Commons Attribution (CC BY) license (<https://creativecommons.org/licenses/by/4.0/>).

## 1. Introduction

Wireless power transfer (WPT) using series–parallel (S-P) resonant coupling is widely used in applications where reliable power transfer through rotating parts is required. It is often used in aviation, robotics, and medicine and in industrial machines as a replacement for slip rings in electrical machines [1,2]. While the use of WPT in medicine, robotics, and less industrially oriented areas is more common, the use of this method within engineering has so far been mainly oriented towards less energy-intensive applications, such as powering diagnostic sensors [3]. The last-mentioned field of application in the engineering industry is related to the unique use of this method enabling the power supply of machining spindle heads intended for angular drilling and angular threading [4].

The use of technological accessories associated with the spindle of an automated machine tool can currently be realized in many ways. In general, there are two ways to connect such accessories. One is to use a spindle head rotation of the machine to operate the technological accessories and the second is to drive accessories externally [5–8].

In the first group, accessories are connected to the spindle of the machine using the standard clamping method, and rotation of the tool is realized via spindle head rotation. For this reason, it is necessary to secure the body of the technological accessory so that it does not rotate together with the spindle head. Among the biggest advantages of this method is the possibility of using automatic tool exchange (hereinafter ATC) and at the same time high power and torque, which is transferred from the spindle of the machine. A drawback of this method is the limited speed of the accessory, which is based on the mechanical nature (planetary gearboxes) of the drive. Furthermore, it is not possible to further position the accessory in the spindle; it is locked in the default position after clamping. However, the necessity of positioning is sometimes necessary for reaching the position in case of machining complicated elements—e.g., drilling and angle tapping. This is important for machining parts in automotive and especially aerospace industry, where usage of lightweight aluminum-based alloys is typical. This type of alloy is characterized by

high cutting speeds, and therefore requires high spindle speed. However, the spindle speed of the above-described accessories is significantly limited due to the mechanical concept.

The second group of accessories is the device, where the spindle of the machine tool is fixed, and the accessory has its own drive. In this case, an external power supply is often used for the drive. The technological spindles driven by their own electric motor reach extreme speeds (even more than 100,000 rpm) and at the same time have sufficient power and torque [9–12]. It is also possible to control the tool speed which is elementary for tapping and threading operations. The machine must adjust the feed in the direction of the tool axis to the spindle speed to match the pitch of the tool. However, the disadvantage is the wiring, which supplies the electric motor from an external source. The wiring reduces the possibility of spindle placement; moreover, the need to connect the cables significantly complicates or even makes ATC impossible [13,14].

Another method that allows simultaneous ATC and positioning of accessories is the pressurized fluid drive. The coolant supplied through the center of the spindle is used for the drive. Accessories using a small turbine to drive the tool achieve high spindle speeds but do not provide sufficient torque or power. On the other hand, attachments fitted with piston hydraulic motors provide sufficient torque but achieve low spindle speeds. However, both solutions do not provide the spindle speed control required for tapping and threading operations.

The above-mentioned limiting factors introduce strong arguments to develop a reliable way of powering the technological accessories of machine tools. As was indicated by the first extensive measurements on an experimental prototype, sufficient power necessary for optimal function can be transferred to the technological accessories in this way, while a further increase in the transmitted power is possible.

Table 1 summarizes the important technological abilities of available solutions for machine tool connection to its accessories.

**Table 1.** Technological abilities of solutions for machine tool connection to its accessories.

Accessory Drive Type	ATC Automatic Tool Exchange	Positioning of Accessories in the Spindle	Power/Torque	Maximum Speed	Speed Control
Driven from machine spindle	Yes	No	High	Medium	Yes
Electric with external source	No	No	High	High	Yes
Cooling liquid turbine drive	Yes	Yes	Low	High	No
Hydro motor drive with coolant	Yes	Yes	Medium	Low	No
Electric with wireless power transfer	Yes	Yes	Medium	Medium	Yes

The main motivation for this work is to use wireless power supply of technological accessories while maintaining the benefits of automatic tool exchange and spindle speed control. Table 1 shows that only a solution with wireless power transmission allows the combination of three key features, namely, ATC capability, the freedom to position accessories around the machine spindle axis, and spindle speed control. In the case of wireless transmission of power to a technological accessory, no power cables prevent the movement of the tool, in addition, it is possible to control the accessory speed and the position of the tool while maintaining the ATC option. A wireless transmission system can also be adopted to provide an independent and fully integrated communication channel necessary for the machine control.

This paper discusses the implementation of the rotary wireless power transfer for machine tool drive using a series–parallel [15–23] resonant inductive coupling. An exhaustive mathematical description of S-P compensation was presented by the authors in [16,18], where a comparison with other basic topologies in terms of resonance capacitor sizes, operating characteristics, and recommendations for the application area is given. An analytical model combining electromagnetic and steady-state modeling for the analysis of the S-P compensated wireless power transmission system for various misalignments is presented in [19]. Another analysis relating to S-P compensation is reported in [20], which compared to [16,17] also provides a flow chart of selection of compensation capacitors for different

topologies and discusses relevant legislation and standards for WPT systems. Some authors support their conclusions using finite element analysis as reported, for example, in [21]. The literature reports numerous works [22,23] dealing with the same issue, but the emphasis is on WPT systems' driving and regulation [24–27].

Although the available literature sources are comprehensive, they mostly present a mathematical apparatus for detailed analysis of existing systems, not a designing or sizing method with possible optimization. The proposed analysis proves the inferential protection of the system against short-circuit failure on the primary side when the load is magnetically separated and when the system is powered from a voltage source. It also indicates the size of the optimal load and recommends the correct location of the operating point on the efficiency characteristic by choosing the mutual inductance. The proposed mathematical description of S-P compensation can also be directly used for the optimal electromagnetic design of coupling elements.

Due to the mechanical stability and the high speed of the rotating parts, the coupling elements are constructed of an iron core made of structural steel, which generates significant losses and thus worsens the quality factors of magnetic couplers. Compared to the power consumption of the entire technological unit, the poorer expected efficiency of wireless transmission means a minor technical issue [28,29]. The significant contribution of this work lies in the relatively simple design of the coupling elements with low cost and considerable robustness, resistance to dynamic conditions, good thermal conductivity, and easy adaptation to any industrial equipment [30–32].

## 2. Description of S-P Compensation Topology

The analyzed S-P topology using first harmonic approximation can be seen in Figure 1. Capacitors  $C_1$  and  $C_2$  represent the compensating capacities of the primary and secondary sides, resistors  $R_1$  and  $R_2$  represent the Joule losses in the windings of the coupling coils  $L_1$  and  $L_2$ , and  $R_L$  is the equivalent resistance characterizing the powered load. Then, the voltage source  $U_1$  represents a mostly complicated circuit solution of the frequency converter. The mentioned topology is dependent on the power level and the target application of the power electronics.

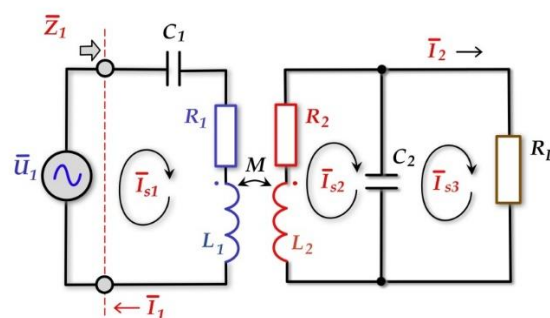


**Figure 1.** Principal schematic of the WPT S-P compensation equivalent circuit.

There are several ways to design a compensation system. First, it is possible to choose the size of the secondary capacitor so that, at the desired resonance frequency, it fully compensates the self-inductance of the secondary coil. A mathematical description based on this approach is provided in detail within Appendix A (A1)–(A21).

The circuit schematic representing the application purpose of the presented solution of the wireless power transfer is shown in Figure 2. Here, the complex power electronic system arrangement is presented, while further mathematical analysis is reflecting system settings considering the detection of the optimal load value vs. maximum system efficiency (A20)–(A22) Appendix A.

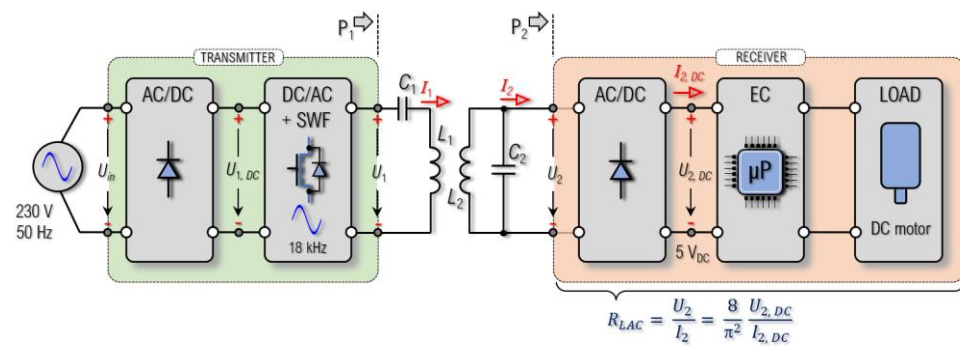


**Figure 2.** Block diagram of system topology; EO denotes any electronic circuits.

The initial conditions and discussion regarding analyses of the system properties are provided in Appendix B.

Based on the mathematical approaches presented in Appendices A and B, the application engineering solution is presented within the following sections, representing the main contribution of this paper, i.e., optimal design of the WPT system for a specific application purpose.

### 3. Design of the WPT System for a Specific Application Prototype

The prototype of the technological accessory contains an annular stator part with a central hole, which is adapted to be attached to the casing of the machine tool spindle, and where the transmitting coil is also located.

The rotor part of the system is equipped with a mechanical interface for attachment to the spindle passing through the central hole of the stator, relative to which it can freely rotate. A receiving coil is also placed on the rotor to supply the DC electric motor driving the spindle (see Figure 3).

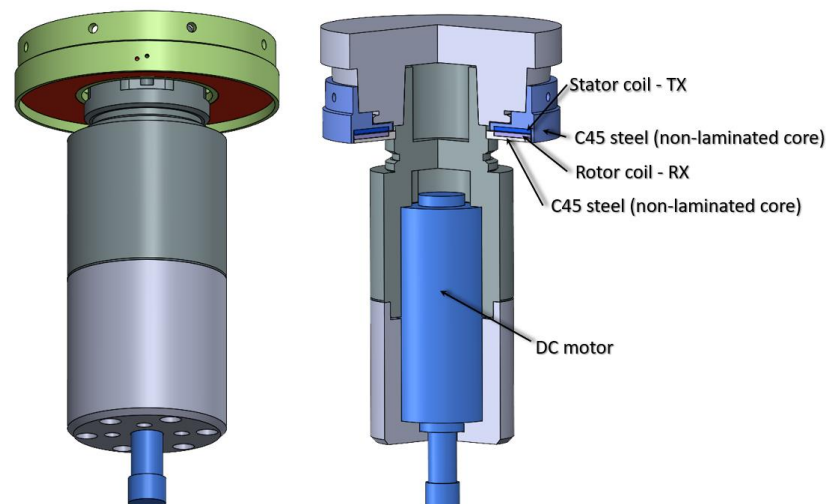


**Figure 3.** CAD model of the technological accessory prototype.

The system's power electronics are designed to power the motor from a voltage source. Since the electric motor represents a load that varies over a wide range, it is necessary to choose such a compensation topology that ensures at least partial resistance (A8) against current overload of the primary in the case of a significant decrease in the load. For this purpose, it is possible to use either some of the derived topologies, e.g., LCC-S or others, or very fast current protection. However, this industrial application prefers robustness (simple design), hence S-P compensation was chosen, offering both partial current protection and voltage source output.

A two-coil arrangement of magnetic couplers is used for power transmission that forms the magnetic field that is stable in space even though the RX rotates. In other words, the magnetic coupling factor  $k$  is constant under all operation modes. The magnetic field is guided through the magnetic poles used at the same time as a supporting structure for attachment to the casing of the machine tool spindle. This design, although very robust, is significantly limited in the operating frequency due to the eddy currents induced in the non-laminated magnetic core and increases the power loss. However, the poorer expected efficiency is acceptable compared to the compact and mechanically stable design of the mechanism.

The system powers a 150 W DC motor with possible short-term overload up to 400 W. This reserve will only be used up to 200 W, which is also considered as the projected nominal power. Following the proposed design process (neglecting the power loss in power electronics and the iron core), we manufactured the system prototype with parameters as listed in Table 1. The voltages  $U_1$  and  $U_2$  (in Table 2) denote the rms values of the first harmonic component.

**Table 2.** Electrical parameters of the designed prototype.

Parameter	Explanation	Value
$U_1, U_2$	System voltages	40 V, 40 V
$P_2$	Transmitted power	200 W
$f_{sv}$	Switching frequency	18 kHz
$k$	Magnetic coupling factor	0.9
$N_1/N_2$	Number of turns	22/20
$L_1/L_2$	Coil inductances	96/78 $\mu$ H
$C_1/C_2$	Compensation capacitances	5.4/1.2 $\mu$ F
$R_1/R_2$	ESR of the coils	0.45/0.45 $\Omega$

The FE model (right) of the resulting prototype (left) is shown Figure 4 and the fabricated magnetic couplers are seen in Figure 5. The Tx and Rx coils are covered with a metallic case with a thickness of 2 mm. From the results of the FE analysis, it is seen that the metallic case avoids saturation under nominal conditions, thus, the side effects of eddy currents and resulting overheating of the system is not expected at all.

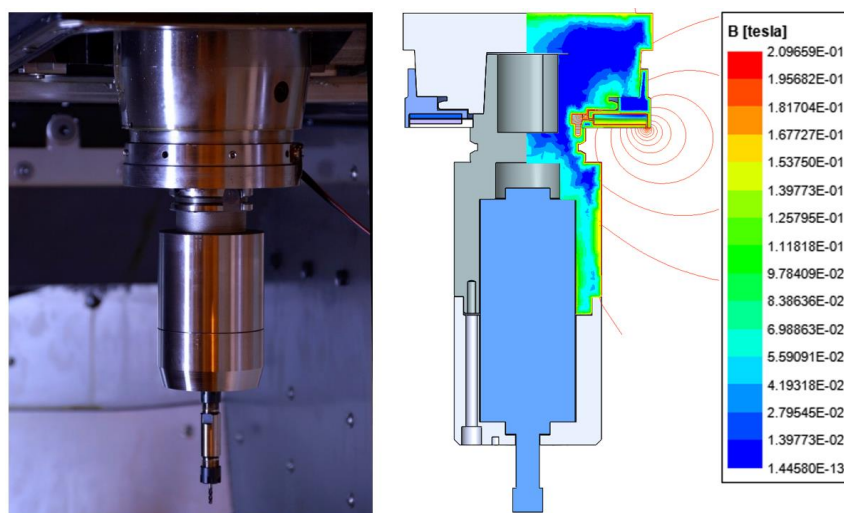


**Figure 4.** FE model (right) of the resulting prototype (left).



**Figure 5.** Magnetic couplers located at the top of the machining spindle clamping head.

#### 4. Design of the WPT System for the Specific Application Prototype

The simplified block diagram of the experimental set up is shown in Figure 6. The measurement was performed without a secondary rectifier; thus, we were able to directly determine the efficiency of the WPT and evaluate the effect of the massive iron core. Due to the losses generated inside the core, the quality factors of TX and RX are low, therefore, the transmitter is powered by a regulated source including a sine-wave filter to reduce THDi as much as possible. The low-inductive load is connected to the receiver. The system efficiency is measured with the precision power meter Yokogawa PX8000 considering the AC-side powers  $P_1$  and  $P_2$ , indicated in Figure 2.

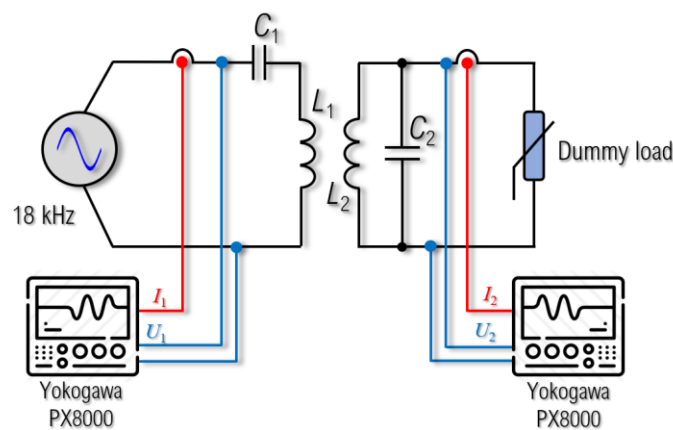


**Figure 6.** Laboratory set up for experimental measurements: test rig (**bottom**) and principal schematic (**top**).

Figures 7 and 8 compare the system quantity waveforms measured for different load values. The oscillograms confirm (A8) that for the optimal load the system operates in resonance with the unity power factor, and for any other load it introduces a phase shift between the supply voltage and current, thus, reducing markedly the system efficiency.

These relations are seen within oscillograms below. Lower loads cause the capacitive character and higher loads cause the inductive character. Summary of the results from these measurements are presented within Table 3. The main focus was on the evaluation of the dependency between the value of the load and system efficiency. For this purpose, using power analyzers, effective values of primary side and secondary side voltages and currents were evaluated. More dependencies received from experimental measurements are shown in Figure 8, where the system efficiency dependency on load and the system efficiency dependency on operational frequency at a constant load are evaluated.



Figure 7. System quantities measured for 2 Ω (left) and 4 Ω (right) of load connected to the secondary voltage.

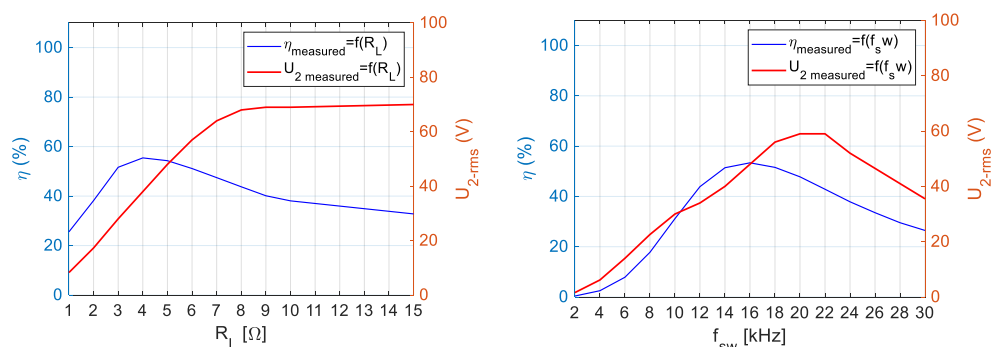


Figure 8. System quantities measured for 6 Ω (left) and 10 Ω (right) of load connected to the secondary voltage.

Table 3. Summary of the experimental measurements.

Load Value $R_L$ (Ω)	Primary Voltage $U_{IRMS}$ (V)	Primary Current $I_{1RMS}$ (A)	Secondary Voltage $U_{2RMS}$ (V)	Secondary Current $I_{2RMS}$ (A)	Efficiency (%)
2	23.965	4.899	8.274	3.853	25.493
4	35.349	4.918	37.338	4.226	54.753
6	53.966	5.000	57.332	4.189	51.222
10	64.848	4.409	65.093	2.821	37.497

In (A16) we showed the existence of an optimal load, which is also proven by Figure 9, left, obtained by increasing the load resistance during the experiment with constant switching frequency. The same figure also confirms (A19), which promises a secondary voltage independent of the load. Because S-P compensation is rather intended for higher load values, it is possible to consider the measured secondary voltage curve starting with a certain value (in this case  $R_L = 8 \Omega$ ) as a constant. The right side of Figure 9 shows the dependence of the secondary voltage and efficiency on the switching frequency.



**Figure 9.** Measurements of system efficiency and secondary voltage as a function of load (**left**) and as a function of switching frequency (**right**) for  $R_L = 8 \Omega$ .

Due to the core losses, it is not possible to achieve a high TX and RX quality factor, and it is therefore advantageous to use a sine filter on the primary side, which will significantly reduce THDi.

The successful operation of the system in an industrial device DMU 40 eVo linear is demonstrated in Figure 10.



**Figure 10.** System successfully operating in an industrial tool DMU 40 eVo linear.

The experiments carried out further indicate the possibility of smooth regulation of the DC motor speed and therefore the power, the possibility of the spindle positioning, and the ability to automatic machining tool replacement.

## 5. Conclusions

As can be seen in (A28), the decisive factor for reaching the highest possible system efficiency will be the maximization of the quality factors, i.e., achieving the maximum inductance and the minimum series resistance of the coils.

The inductance  $L_1$  is not proportional directly to the primary voltage, but to the power of the ratio between the primary and secondary voltages. Therefore, we can use the same system for both lower and higher voltage levels.

By connecting the optimal load (A14) to the terminals of the system, the highest transmission efficiency is achieved. Since the speed of efficiency growth while increasing the load is greater for  $R_L \leq R_{L-opt}$  than the speed of its decrease for  $R_L > R_{L-opt}$ , the secondary goal of the design it therefore to meet the condition  $R_L \geq R_{L-opt}$ .

The last important feature of S-P compensation is its frequency intolerance. It is clear from Equation (A8) that the system is in a state of full resonance only for a specific (designed) load. Any deviation from this point will cause the system to detune and lower its power factor, which, as a side effect, can be used as inherent current protection.

The experiments carried out indicated the possibility of smooth regulation of the DC motor speed and therefore the power, the possibility of the spindle positioning, and the ability to automate machining tool replacement. The proposed design is easy to

manufacture and has low production costs. Furthermore, it is characterized by considerable robustness, resistance to dynamic conditions, and easy adaptation to any other industrial equipment. All these arguments represent very significant technical advantages important for this industrial application area.

**Author Contributions:** Conceptualization, formal analysis, supervision, and writing—original draft, V.K.; investigation and writing—original draft, J.S., methodology and investigation, T.K. and M.K.; software and investigation, J.H.; writing—review and editing, M.F. All authors have read and agreed to the published version of the manuscript.

**Funding:** This research has been supported by the Ministry of Education, Youth and Sports of the Czech Republic under the project OP VVV Electrical Engineering Technologies with High-Level of Embedded Intelligence CZ.02.1.01/0.0/0.0/18\_069/0009855, and under the project Long-term conceptual development of Regional Technological Institute.

**Data Availability Statement:** Not applicable.

**Acknowledgments:** The authors would like to thank for project funding granted by VEGA 1/0593/20.

**Conflicts of Interest:** The authors declare no conflict of interest.

## Appendix A. Analyses of the S-P Compensation System Targeting Optimal System Efficiency

The resonant frequency of the system described in Figure 1 is defined by the well-known Thomson relationship (A1).

$$f_{01} = \frac{1}{2\pi\sqrt{LC}}, \quad \omega = 2\pi f_{01} \quad (\text{A1})$$

The primary capacitor is then sized to compensate for the net reflecting inductance of the entire circuit. This gives a power factor equal to one.

$$C_2 = \frac{1}{\omega^2 L_2} \quad (\text{A2})$$

The size of primary capacitor is then provided using condition (A3).

$$\Im\{\bar{Z}_1\} = 0 \quad (\text{A3})$$

where  $\bar{Z}_1$  is the total impedance of the circuit (see Figure 1). The system can be described by a system of three equations (A4).

$$\begin{bmatrix} \bar{I}_{S1} \\ \bar{I}_{S2} \\ \bar{I}_{S3} \end{bmatrix} = \begin{bmatrix} R_1 + j\left(\omega L_1 - \frac{1}{\omega C_1}\right) & -j\omega M & 0 \\ -j\omega M & R_2 + j\left(\omega L_2 - \frac{1}{\omega C_2}\right) & \frac{j}{\omega C_2} \\ 0 & \frac{j}{\omega C_2} & R_L - \frac{j}{\omega C_2} \end{bmatrix}^{-1} \begin{bmatrix} \bar{U}_1 \\ 0 \\ 0 \end{bmatrix} \quad (\text{A4})$$

$$\begin{aligned} \bar{I}_1 &= \bar{I}_{S1} \\ \bar{I}_2 &= \bar{I}_{S3} \end{aligned} \quad (\text{A5})$$

In this case, it will be preferable to use the condition (A6) instead of the condition (A3) for deriving primary capacity, which, however, leads to the numerically identical result.

$$\Im\{\bar{I}_1\} = 0 \quad (\text{A6})$$

The solution is (A7).

$$C_1 = \frac{R_2^2 R_L^2 + R_2^2 L_2^2 \omega^2 + 2\omega^2 L_2^2 R_2 R_L + \omega^4 L_2^4}{\omega^2 (L_1 R_2^2 R_L^2 + L_1 L_2^2 R_2^2 \omega^2 + 2L_1 \omega^2 L_2^2 R_2 R_L + L_1 \omega^4 L_2^4 - L_2^3 \omega^4 M^2)} \quad (\text{A7})$$

If  $M = k\sqrt{L_1L_2}$ , then the Equation (A7) changes into (A8).

$$C_1 = \frac{1}{\omega^2L_1} - \frac{k^2\omega^4L_2^4}{\omega^2L_1[\omega^4L_2^4(k^2 - 1) - \omega^2L_2^2R_2(R_2 + 2R_L) - R_2^2R_L^2]} \tag{A8}$$

The Equation (A8) shows that the full resonance of the system can be achieved only for one specific load. Any change in it leads to frequency tuning of the system, which is not necessarily an inappropriate procedure. For example, this is advantageous for low-cost electronics solutions without feedback regulation.

From the Equation (A8), it is obvious that the size of the primary capacity can be determined only by knowledge of the electrical elements of the whole circuit, i.e., only as the last value.

An important parameter of the system is probably the efficiency, which can be determined from the power-to-power ratio according to (A9).

$$\eta = \frac{P_2}{P_1} = \frac{R_L|\bar{I}_2|^2}{\Re\{\bar{U}_1\bar{I}_1^*\}} \tag{A9}$$

Both the power input and the power of Equation (A9) are rather confusing relations in the given state, which can be simplified by applying conditions (A2) and (A7).

The powers are then as (A10) and (A11).

$$P_1 = \frac{U_1^2[R_2^2R_L^2 + L_2^2R_2(R_2 + 2R_L)\omega^2 + L_2^2\omega^4]}{R_1R_2^2R_L^2 + \omega^2R_2[M^2R_L^2 + L_2^2R_1(R_2 + 2R_L)] + \omega^4L_2^2[L_2^2R_1 + M^2(R_2 + R_L)]} \tag{A10}$$

$$P_2 = \frac{L_2^2M^2U_1^2\omega^4R_L[R_2^2R_L^2 + L_2^2R_2(R_2 + 2R_L)\omega^2 + L_2^2\omega^4]}{(R_1R_2^2R_L^2 + R_2[M^2R_L^2 + L_2^2R_1(R_2 + 2R_L)])\omega^2 + L_2^2[L_2^2R_1 + M^2(R_2 + R_L)]\omega^4}^2 \tag{A11}$$

Putting them back into Equation (A9) we get (A12).

$$\eta = \frac{M^2\omega^4L_2^2R_L}{R_1R_2^2R_L^2 + R_2[M^2R_L^2 + L_2^2R_1(R_2 + 2R_L)]\omega^2 + L_2^2[L_2^2R_1 + M^2(R_2 + R_L)]\omega^4} \tag{A12}$$

The optimal load in terms of efficiency can be determined from the first derivative (A13) according to the load, which we put equal to zero. We obtain two solutions, of which only (A13) makes physical sense.

$$\frac{d\eta}{dR_L} = 0 \Rightarrow R_{L-opt} = \frac{j\omega L_2\sqrt{R_1R_2^2 + (L_2^2R_1 + M^2R_2)\omega^2}}{\sqrt{-R_2(R_1R_2 + M^2\omega^2)}} \tag{A13}$$

In the denominator (A13) there is a negative number below the square root, which makes an imaginary unit appear in the numerator. By taking the power operation and taking the square root back, we can comfortably get into a more usual shape (A14).

$$R_{L-opt} = \sqrt{\left(\frac{j\omega L_2\sqrt{R_1R_2^2 + (L_2^2R_1 + M^2R_2)\omega^2}}{\sqrt{-R_2(R_1R_2 + M^2\omega^2)}}\right)^2} = \omega L_2\sqrt{\frac{R_1R_2^2 + (L_2^2R_1 + M^2R_2)\omega^2}{R_2(R_1R_2 + M^2\omega^2)}} \tag{A14}$$

The theoretical maximum efficiency (A15) can be found by employing (A14) back into (A12).

$$\eta_{MAX} = \frac{\omega^4L_2^2M^2}{2R_2(R_1R_2 + M^2\omega^2)\omega L_2\sqrt{\frac{R_1R_2^2 + (L_2^2R_1 + M^2R_2)\omega^2}{R_2(R_1R_2 + M^2\omega^2)}} + L_2^2\omega^2(2R_1R_2 + M^2\omega^2)} \tag{A15}$$

Formal comparisons of (A14) and (A15) result in (A16).

$$\eta_{MAX} = \frac{\omega^4 L_2^2 M^2}{2R_2(R_1 R_2 + M^2 \omega^2) R_{L-opt} + \omega^2 L_2^2 (2R_1 R_2 + M^2 \omega^2)} \quad (A16)$$

The main goal is to design the electrical parameters of the coupling elements so that the specified power output is achieved at the given supply voltage and frequency. For practical reasons, it is good to first derive the amount of voltage on the load (A17).

$$|\bar{U}_2| = R_L |\bar{I}_2| = R_L \sqrt{(\Re\{\bar{I}_2\})^2 + (\Im\{\bar{I}_2\})^2} \quad (A17)$$

If we apply (A2) and (A7) again, we get (A18).

$$|\bar{U}_2| = \sqrt{\frac{L_2^2 M^2 U_1^2 \omega^4 [R_2^2 R_L^2 + L_2^2 R_2 (R_2 + 2R_L) \omega^2 + L_2^2 \omega^4] R_L^2}{(R_1 R_2^2 R_L^2 + R_2 [M^2 R_L^2 + L_2^2 R_1 (R_2 + 2R_L)] \omega^2 + L_2^2 [L_2^2 R_1 + M^2 (R_2 + R_L)] \omega^4)^2}} \quad (A18)$$

Considering zero  $I^2R$  losses, (A18) takes new form (A19).

$$|\bar{U}_2|_{\Delta P=0} = U_1 \frac{L_2}{M} = \frac{U_1}{k} \sqrt{\frac{L_2}{L_1}} \quad (A19)$$

With operational parameters  $U_1$ ,  $U_2$ ,  $P_2$ , and  $f$  it is possible to estimate the required mutual inductance  $M$ .

First, we determine the load resistance (A20),

$$R_L = \frac{U_2^2}{P_2} \quad (A20)$$

which we subsequently substitute back into (A18) while obtaining the important design parameter (A21). Attention must be paid to sizing the operating load (A20), which should be equal to or greater than the optimal load (A14).

$$M = \sqrt{\frac{\sqrt{M_a} - M_b}{M_c}} \quad (A21)$$

A substitution for (A21) is provided in (A22).

$$\begin{aligned} M_a &= L_2^2 R_2^2 U_1^2 \omega^6 [\omega^2 L_2^2 (R_L^2 U_1^2 - 4U_2^2 (R_2 + R_L)) - 4U_2^2 R_1 R_2 R_L^2] [R_2^2 R_L^2 + L_2^2 R_2 (R_2 + 2R_L) \omega^2 + L_2^4 \omega^4]^2 \\ M_b &= \omega^2 [2U_2^2 R_1 R_2 R_L^2 + \omega^2 L_2^2 (2U_2^2 R_1 (R_2 + R_L) - R_L^2 U_1^2)] [R_2^2 R_L^2 + L_2^2 R_2 (R_2 + 2R_L) \omega^2 + \omega^4 L_2^4]^2 \\ M_c &= 2\omega^4 [U_2 R_2 R_L^2 + L_2^2 U_2 (R_2 + R_L) \omega^2]^2 \end{aligned} \quad (A22)$$

To substitute into (A21) we only need to determine (choose) the size of the secondary coil parameters. Based on the geometrical dimensions of the coupling coils used in FEA, we can further estimate the magnetic coupling factor  $k$  from which the self-inductance of the primary is easily calculated by rearranging  $M = k\sqrt{L_1 L_2}$ . Capacitors are then designed based on (A2) and (A8). The Equation (A15) verifies the ability to reach high efficiency.

## Appendix B. System Properties Discussion

Let us first consider Equation (A15). This equation provides the maximum possible efficiency when considering the Joule losses (here  $R_1$  and  $R_2$ ) in the winding.

It is important to note that the model assumes amplitude, and since the active power (A23) is the mean value of the product of voltage and current, the design power must be taken as twice the required power.

In general, the aim when designing a system is to ensure the smallest possible energy losses. We can therefore expect the product  $R_1 R_2$  to take on very small numbers. Therefore, for simplicity, we declare  $R_1 R_2 = 0$ , which converts the Equation (A15) into the form (A23).

$$\eta_{MAX} \approx \frac{\omega^2 L_2^2}{2R_2 \sqrt{\omega^2 L_2^2 \left(1 + \frac{L_2^2 R_1}{M^2 R_2}\right)} + L_2^2 \omega^2} \quad (A23)$$

The equation is further simplified to the form of identity applications  $k\sqrt{L_1 L_2}$ .

$$\eta_{MAX} \approx \frac{1}{2R_2 \sqrt{\omega^2 L_2^2 \left(1 + \frac{L_2^2 R_1}{k^2 M^2 R_2}\right)} + \omega^2 L_2^2} \quad (A24)$$

Resonant circuits are usually described by quality factors  $Q_{1,2} = \frac{\omega L_{1,2}}{R_{1,2}}$ . By using them in (A24), we obtain (A25)

$$\eta_{MAX} \approx \frac{1}{1 + 2\sqrt{\frac{1}{k^2 Q_1 Q_2} + \frac{1}{Q_2^2}}} \quad (A25)$$

As can be seen from the result, the decisive factor here will be the maximization of the quality factors, i.e., at the given frequency we want to achieve the maximum inductance and the minimum series resistance of the coils.

Considering zero losses of both coils will simplify (A21) into (A26).

$$M = \frac{U_1}{U_2} L_2 \Rightarrow L_1 = \frac{L_2}{k^2} \frac{U_1^2}{U_2^2} \quad (A26)$$

The equation shows that the inductance  $L_1$  is not proportional to the primary voltage, as is the case, for example, with S-S compensation [8,9], but to the power of the ratio of the primary and secondary voltages. Therefore, we can use the same system for both lower and higher voltage levels, with the condition that the ratio of these voltages must be the same.

An equally important feature results from Equation (A12), which indicates the relationship between efficiency and load.

From the previous considerations, by connecting the optimal load (A14) to the terminals of the system, the highest transmission efficiency is achieved. However, the question remains how the system behaves at the surrounding operating points. In Equation (A12) it can be directly seen that the efficiency will be zero when  $R_L = 0$ . Likewise, we obtain zero efficiency (A27) even in the case of the second extreme, when  $R_L \rightarrow \infty$ .

$$\lim_{R_L \rightarrow \infty} \eta_{eq.(12)} = 0 \quad (A27)$$

The original Equation (A12) is formed by substituting (A28) for  $R_L$ .

$$R_L = \frac{r}{R_{L-opt}} = \frac{r}{\omega L_2 \sqrt{\frac{R_1 R_2^2 + (L_2^2 R_1 + M^2 R_2) \omega^2}{R_2 (R_1 R_2 + M^2 \omega^2)}}} \quad (A28)$$

Then, the equation can take the form

$$\eta = \frac{k_1 r}{k_2 (k_3 + k_4 r^2 + k_5 r)} \quad (A29)$$

where constants  $k_1 \div k_5$  are stated in the Equation (A30)

$$\begin{aligned} k_1 &= L_2 M^2 \omega^3 \sqrt{R_2 (R_1 R_2 + M^2 \omega^2)} \\ k_2 &= \sqrt{R_1 R_2^2 + (R_1 L_2^2 + M^2 R_1) \omega^2} \\ k_3 &= L_2^4 R_1 \omega^4 + L_2^2 R_2 \omega^2 (R_1 R_2 + M^2 \omega^2) \\ k_4 &= \frac{R_2^2 (R_1 R_2 + M^2 \omega^2)^2}{\omega^2 L_2^2 [R_1 R_2^2 + (L_2^2 R_1 + M^2 R_2) \omega^2]} \\ k_5 &= \frac{\omega L_2 \sqrt{R_2 (R_1 R_2 + M^2 \omega^2)} (2 R_1 R_2 + M^2 \omega^2)}{\sqrt{R_1 R_2^2 + (L_2^2 R_1 + M^2 R_2) \omega^2}} \end{aligned} \quad (\text{A30})$$

Regardless of the complexity of these relationships, it is appropriate to focus only on Equation (A28). It physically behaves the same as (A12), with the difference that  $r$  is a relative quantity. For  $r = 1$ , the result will be the same as we find from (A15), i.e., the theoretically maximum achievable efficiency. It is therefore obvious that from zero  $r$  the efficiency will rise to a maximum value (for  $r = 1$ ), and from this point onwards the efficiency will only decrease. As proved by (A13), this determined the only extremum of the function.

Considering (A29) for low values of  $r$ , i.e.,  $r \ll 1$ , it is possible to neglect the term  $k_4 r^2$  and the result is an almost linearly increasing function, the derivative of which gradually decreases with the value of  $r$ . With higher values of  $r$ , on the other hand, the equation takes the form of a certain type of hyperbola, which, however, has a much slower trend than the increasing part of the original function. The secondary goal of the design will therefore be a circuit for which the ratio  $R_L \geq R_{L-opt}$  would apply.

The last important feature of S-P compensation is its frequency intolerance.

It is clear from (A8) that the system is in a state of full resonance only for a specific designed load. Any deviation from this starting point will cause the system to detune and lower its power factor. As shown above, when the load is uncoupled ( $k = 0$ ), the primary capacitance from (A8) would need to be designed for the resonance condition.

In that case, the circuit is not at resonance and the drawn current is limited by the mutual reactance of the circuit. This property therefore acts as an inherent current protection. A similar effect can also be achieved in the case of an infinitely large value of the load; here, it is necessary to determine the limit from (A7), i.e., (A31).

$$\lim_{R_L \rightarrow \infty} C_{1-eq. (7)} = C_{1(R_L \rightarrow \infty)} = \frac{1}{\omega^2 L_1} \quad (\text{A31})$$

The extremum of the function was found with the help of (A7) or (A8). The second extremum is obtained by substituting the condition  $R_L = 0$  into (A7). The result is provided in (A32), which is numerically higher than that obtained from (A31).

$$C_{1(R_L=0)} = \frac{R_2^2 + \omega^2 L_2^2}{\omega^2 L_1 R_2^2 + L_1 (L_1 L_2 - M^2) \omega^4} \quad (\text{A32})$$

This fact is also confirmed by a closer analysis of (A7), where we describe a continuously decreasing function passing through points (A32), (A8), and (A31).

The percentage difference (A33) of capacities for both extreme cases can be obtained using the ratio of (A32) and (A31).

$$\frac{C_{1(R_L=0)}}{C_{1(R_L \rightarrow \infty)}} = \frac{L_1 (R_2^2 + L_2^2 \omega^2)}{L_1 R_2^2 + L_2 (L_1 L_2 - M^2) \omega^2} \approx \frac{L_1 L_2}{L_1 L_2 - M^2} \approx \frac{1}{1 - k^2} \quad (\text{A33})$$

It can be seen from the above equations that by reducing the coupling factor  $k$ , the frequency circuit is partially stabilized.

## References

1. Bastiaens, K.; Krop, D.C.J.; Curti, M.; Jumayev, S.; Lomonova, E.A. Design of a High-Frequency Wireless Power Transfer System for a Rotating Application. In Proceedings of the 19th International Symposium on Electromagnetic Fields in Mechatronics, Electrical and Electronic Engineering (ISEF), Nancy, France, 29–31 August 2019.
2. Xia, Q.; Yan, L. Application of wireless power transfer technologies and intermittent energy harvesting for wireless sensors in rotating machines. *Wirel. Power Transf.* **2016**, *3*, 93–104. [[CrossRef](#)]
3. Garraud, A.; Jimenez, J.D.; Garraud, N.; Arnold, D. Electrodynamics wireless power transmission to rotating magnet receivers. *J. Phys. Conf. Ser.* **2014**, *557*, 012136. [[CrossRef](#)]
4. Madzharov, N.; Ilarionov, R.; Petkov, V.; Petkov, L. Inductive Power Transfer Systems for Rotating Applications. In Proceedings of the PCIM Europe 2018, International Exhibition and Conference for Power Electronics, Intelligent Motion, Renewable Energy and Energy Management, Nurnberg, Germany, 5–7 June 2018; pp. 1–8.
5. Legranger, J.; Friedrich, G.; Vivier, S.; Mipo, J.C. Comparison of Two Optimal Rotary Transformer Designs for Highly Constrained Applications. In Proceedings of the 2007 IEEE International Electric Machines Drives Conference, Antalya, Turkey, 3–5 May 2007; Volume 2, pp. 1546–1551.
6. Niu, M.; Sun, X.; Ma, H.; Zhu, Z.; Huang, T.; Song, K. Analysis and Design of Wireless Power Transfer System for Rotational Inertial Navigation Application. *Appl. Sci.* **2022**, *12*, 6392. [[CrossRef](#)]
7. Kikuchi, S.; Sakata, T.; Takahashi, E.; Kanno, H. Development of wireless power transfer system for robot arm with rotary and linear movement. In Proceedings of the 2016 IEEE International Conference on Advanced Intelligent Mechatronics (AIM), Banff, AB, Canada, 12–15 July 2016.
8. Lee, G.; Gwak, H.; Kim, Y.-S.; Park, W.-S. Wireless power transfer system for diagnostic sensor on rotating spindle. In Proceedings of the 2013 IEEE Wireless Power Transfer (WPT), Perugia, Italy, 15–16 May 2013.
9. Qiao, X.; Niu, S.; Lin, J.; Chen, M.; Wu, Y. A Novel Magnetically Coupled Resonant Wireless Power Transfer Technique Used in Rotary Ultrasonic Machining Process. In Proceedings of the 2021 IEEE Wireless Power Transfer Conference (WPTC), San Diego, CA, USA, 1–4 June 2021; pp. 1–4. [[CrossRef](#)]
10. Ben Brahim, S.; Bouallegue, R.; David, J.; Vuong, T.H.; David, M. A Wireless On-line Temperature Monitoring System for Rotating Electrical Machine. *Wirel. Pers. Commun.* **2017**, *95*, 979–999. [[CrossRef](#)]
11. Pang, D.-C.; Wang, C.-T. A Wireless-Driven, Micro, Axial-Flux, Single-Phase Switched Reluctance Motor. *Energies* **2018**, *11*, 2772. [[CrossRef](#)]
12. Ben Brahim, S.; Bouallegue, R.; David, J.; Vuong, T.H.; David, M. Design and implementation of wireless sensor network node for rotating electrical machine. In Proceedings of the 2016 IEEE Symposium on Computers and Communication (ISCC), Messina, Italy, 27–30 June 2016; pp. 738–742. [[CrossRef](#)]
13. Zhang, W.; Mi, C.C. Compensation Topologies of High-Power Wireless Power Transfer Systems. *IEEE Trans. Veh. Technol.* **2016**, *65*, 4768–4778. [[CrossRef](#)]
14. Aydin, E.; Aydemir, M.T.; Aksoz, A.; El Baghdadi, M.; Hegazy, O. Inductive Power Transfer for Electric Vehicle Charging Applications: A Comprehensive Review. *Energies* **2022**, *15*, 4962. [[CrossRef](#)]
15. Villa, J.L.; Sallan, J.; Osorio, J.F.S.; Llombart, A. High-Misalignment Tolerant Compensation Topology for ICPT Systems. *IEEE Trans. Ind. Electron.* **2012**, *59*, 945–951. [[CrossRef](#)]
16. Shevchenko, V.; Husev, O.; Strzelecki, R.; Pakhaliuk, B.; Poliakov, N.; Strzelecka, N. Compensation Topologies in IPT Systems: Standards, Requirements, Classification, Analysis, Comparison and Application. *IEEE Access* **2019**, *7*, 120559–120580. [[CrossRef](#)]
17. Wang, Y.; Zhang, H.; Lu, F. Review, Analysis, and Design of Four Basic CPT Topologies and the Application of High-Order Compensation Networks. *IEEE Trans. Power Electron.* **2022**, *37*, 6181–6193. [[CrossRef](#)]
18. Sohn, Y.H.; Choi, B.H.; Lee, E.S.; Lim, G.C.; Cho, G.-H.; Rim, C.T. General Unified Analyses of Two-Capacitor Inductive Power Transfer Systems: Equivalence of Current-Source SS and SP Compensations. *IEEE Trans. Power Electron.* **2015**, *30*, 6030–6045. [[CrossRef](#)]
19. Kushwaha, B.K.; Rituraj, G.; Kumar, P.; Bauer, P. Mathematical model for the analysis of series–parallel compensated wireless power transfer system for different misalignments. *IET Circuits Devices Syst.* **2019**, *13*, 970–978. [[CrossRef](#)]
20. Ahire, D.; Gond, V.J.; Chopade, J.J. Compensation topologies for wireless power transmission system in medical implant applications: A review. *Biosens. Bioelectron. X* **2022**, *11*, 100180. [[CrossRef](#)]
21. Rehman, M.; Nallagownden, P.; Baharudin, Z. Efficiency investigation of SS and SP compensation topologies for wireless power transfer. *Int. J. Power Electron. Drive Syst.* **2019**, *10*, 2157–2164. Available online: <https://www.proquest.com/scholarly-journals/efficiency-investigation-ss-sp-compensation/docview/2323175597/se-2> (accessed on 17 August 2022). [[CrossRef](#)]
22. Hou, J.; Chen, Q.; Zhang, L.; Xu, L.; Wong, S.-C.; Tse, C.K. Compact Capacitive Compensation for Adjustable Load-Independent Output and Zero-Phase-Angle Input for High Efficiency IPT Systems. *IEEE J. Emerg. Sel. Top. Power Electron.* **2022**, *10*, 4923–4936. [[CrossRef](#)]
23. Song, K.; Li, Z.; Jiang, J.; Zhu, C. Constant Current/Voltage Charging Operation for Series–Series and Series–Parallel Compensated Wireless Power Transfer Systems Employing Primary-Side Controller. *IEEE Trans. Power Electron.* **2018**, *33*, 8065–8080. [[CrossRef](#)]
24. Jia, J.; Jia, Y.; Li, X. Analysis, Design, and Experimental Verification of a Parallel Wireless Power and Data Transmission Method for Rotary Steering Systems. *Energies* **2022**, *15*, 6349. [[CrossRef](#)]

25. Qiao, K.; Rong, E.; Sun, P.; Zhang, X.; Sun, J. Design of LCC-P Constant Current Topology Parameters for AUV Wireless Power Transfer. *Energies* **2022**, *15*, 5249. [[CrossRef](#)]
26. Zhang, L.; Li, H.; Guo, Q.; Xie, S.; Yang, Y. Research on Constant Voltage/Current Output of LCC-S Envelope Modulation Wireless Power Transfer System. *Energies* **2022**, *15*, 1562. [[CrossRef](#)]
27. Wang, K.; Zuo, Z.; Sang, L.; Zhu, X. Comprehensive Analysis for Electromagnetic Shielding Method Based on Mesh Aluminium Plate for Electric Vehicle Wireless Charging Systems. *Energies* **2022**, *15*, 1546. [[CrossRef](#)]
28. Ueda, K.; Inoue, Y.; Morimoto, S.; Sanada, M. Characteristic Comparison of Three-Phase Wireless Power Transfer at 85 kHz Using a Rotating Coordinate System. In Proceedings of the 2020 23rd International Conference on Electrical Machines and Systems (ICEMS), Hamamatsu, Japan, 24–27 November 2020; pp. 1779–1783. [[CrossRef](#)]
29. Song, S.; Zhang, W.; Jin, Z.; Geng, Q. Analysis of S-S Resonance Compensation Circuit of Electric Vehicle Wireless Power Transfer System. In Proceedings of the 2020 IEEE 4th Conference on Energy Internet and Energy System Integration (EI2), Wuhan, China, 30 October–1 November 2020; pp. 619–622. [[CrossRef](#)]
30. Hagen, S.; Knippel, R.; Dai, J.; Ludois, D.C. Capacitive coupling through a hydrodynamic journal bearing to power rotating electrical loads without contact. In Proceedings of the 2015 IEEE Wireless Power Transfer Conference (WPTC), Boulder, CO, USA, 13–15 May 2015; pp. 1–4. [[CrossRef](#)]
31. Ludois, D.C.; Frankforter, K. A Rotating Double Layer Capacitive Slip Ring Concept for Power & Heat Transfer in Machines using an Ionic Conducting Working Fluid. In Proceedings of the 2020 IEEE Energy Conversion Congress and Exposition (ECCE), Detroit, MI, USA, 11–15 October 2020; pp. 4238–4245. [[CrossRef](#)]
32. Quiroz, C.H.; Oquena, E.Q.; Castano, J.C. Design of a Wireless Thermal on-Line Monitoring System for Rotating Electrical Machines. In Proceedings of the 2012 VI Andean Region International Conference, Cuenca, Ecuador, 7–9 November 2012; p. 229. [[CrossRef](#)]